Copyright
by
Jonathan Michael Ashley
2014

The Report committee for Jonathan Michael Ashley
Certifies that this is the approved version of the following report:

# Closed-loop Control of Shock Location to Prevent Hypersonic Inlet Unstart

APPROVED BY

SUPERVISING COMMITTEE:

Maruthi R. Akella, Supervisor

Noel T. Clemens

# Closed-loop Control of Shock Location to Prevent Hypersonic Inlet Unstart

**by**

**Jonathan Michael Ashley, B.S.**

**THESIS**

Presented to the Faculty of the Graduate School of

The University of Texas at Austin

in Partial Fulfillment

of the Requirements

for the Degree of

**MASTER OF SCIENCE IN ENGINEERING**

THE UNIVERSITY OF TEXAS AT AUSTIN

August 2014

To my family and friends

# Closed-loop Control of Shock Location to Prevent Hypersonic Inlet Unstart

Jonathan Michael Ashley, M.S.E.
The University of Texas at Austin, 2014

Supervisor: Maruthi R. Akella

Hypersonic inlet unstart remains a major technical obstacle in the successful implementation of hypersonic air-breathing propulsion systems such as ramjets and scramjets. Unstart occurs when combustor-induced pressure fluctuations lead to rapid expulsion of the shock system from the isolator, and is associated with loss of thrust. The research presented here attempts to mitigate this behavior through the design and implementation of a closed-loop control scheme that regulates shock location within a Mach 1.8 wind tunnel isolator test section. To localize the position of the shock within the isolator, a set of high frequency Kulite pressure transducers are used to measure the static pressure at various points along the wind tunnel test section. A novel Kalman filter based approach is utilized, which fuses the estimates from two distinct shock localization algorithms running at 250 Hz to determine the location of the shock in real time. The primary shock localization algorithm is a geometrical shock detection scheme that can estimate the position of the shock system even when it is located between pressure transducers. The second algorithm utilizes a sum-of-pressures technique that can be calibrated by

the geometrical algorithm in real time. The closed-loop controller generates commands every 100 ms to actuate a motorized flap downstream of the test section in an effort to regulate the shock to the desired location. The closed-loop control implementation utilized a simple logic-based controller as well as a Proportional-Integral (PI) and a Proportional-Derivative (PD) Controller. In addition to the implementation of control algorithms, the importance of various design criteria necessary to achieve satisfactory control performance is explored including parameters such as pressure transducer spacing, shock localization speed, flap-motor actuation speed and actuator resolution. Experimental results are presented for various test scenarios such as regulation of the shock location in the presence of stagnation pressure disturbances as well as tracking of time-varying step inputs. Performance and robustness properties of the tested control implementations are discussed. Further areas of improvement for the closed-loop control system in both hardware and software are discussed, and the need for reduced-order dynamics-based controllers is presented.

# Table of Contents

# List of Figures

# Chapter 1

# Introduction

The advancement of hypersonic air-breathing propulsion technology makes possible a future of efficient high-speed air travel and low-cost access to space. The successful development of hypersonic propulsion systems such as ramjets and scramjets will allow aircraft to operate at speeds ranging from Mach 2.5 to Mach 12 without the need to carry additional oxidizer. These vehicles may even be able to reach speeds up to Mach 24 with the use of additional oxidizer [2]. Before these technologies can be widely adopted and integrated into vehicle designs, many technical challenges remain to be overcome. One of the most difficult obstacles remaining is the challenge of preventing hypersonic inlet unstart.

## 1.1 Ramjet/Scramjet Operation

A ramjet is a type of jet engine that contains no compressor or turbine. It relies on its forward velocity to force air through the engine. As air enters the engine, it is compressed by the inlet geometry until the flow conditions become subsonic. Fuel is then injected and ignited in the combustor after which the air is expanded out of the nozzle producing thrust. As a result of this configuration, ramjets have many advantages over conventional turbojet

engines such as lower cost, lower weight, and higher allowable combustion temperatures.

Most ramjets are designed to operate efficiently at supersonic speeds (Mach 2.5 to Mach 5) which makes them relatively inefficient for subsonic use [2]. As a result, most ramjet vehicles must be initially accelerated to supersonic speeds via a rocket or some other form of propulsion before ramjet operation can commence.

Inlet and isolator design is a crucial aspect in the development of a ramjet engine. The inlet must be carefully designed to recover as much total pressure from the flow during the compression process which occurs through a series of oblique shocks in the isolator terminating with a normal shock which yields a subsonic flow [2].

A scramjet is formally known as a "supersonic combustion ramjet." It is very similar to a traditional ramjet, but has one major distinction that the flow remains supersonic throughout the entire engine. Figure 1.1 displays the anatomy of a typical scramjet [1].

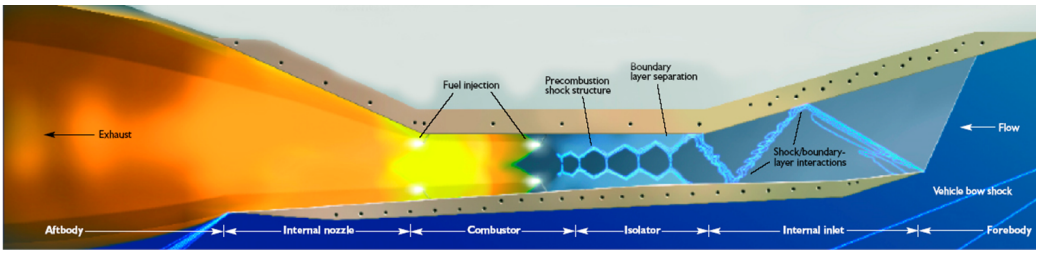


Figure 1.1: Scramjet Diagram (Courtesy of Dean Andreadis [1])

A scramjet is capable of much higher speeds (Mach 10-12) than a ramjet because it does not completely decelerate the flow to subsonic speeds using a

normal shock. This prevents extremely high temperatures from occurring in the combustor which would otherwise lead to fuel dissociation.

To increase the versatility and operational range of these forms of propulsion technology, dual-mode scramjets have been designed that allow the engine to operate in both ramjet and scramjet modes. This would allow a hypersonic vehicle more versatility by granting it a larger range of operational speeds. For this propulsion system to succeed, the shock structure located in the isolator must be regulated such that the engine does not unstart when operating in ramjet or scramjet mode.

## 1.2 Inlet Unstart

Inlet unstart is a phenomenon in which various pressure disturbances can cause the shock structure located in the isolator of the ramjet or scramjet to become disgorged from the inlet. These pressure disturbances can be the result of stagnation pressure variations or oscillations in the combustor pressure as a result of uneven combustion or poor control of fuel injection rate. This unintended displacement of the shock structure leads to a loss of compression in the flow and subsequently causes a loss of thrust in the engine that is often catastrophic.

## 1.3 Related Work

A large amount of research has been previously conducted on the topic of inlet unstart. This work has approached various aspects of the problem rang-

ing from characterizing the dynamics of unstart to full experimental demonstration of closed-loop control of shock location.

Past experiments conducted on a scramjet inlet-isolator model in a Mach 5 flow have shown a link between inlet unstart and boundary layer separation in the isolator [3]. Furthermore, several oscillatory unstart modes were observed with varying amplitudes and frequencies of oscillation. This research suggests that control of boundary layer separation may serve as a suitable method of actuation to prevent inlet unstart. For this reason, vortex generators were considered as a possible actuation method as they have been shown to help prevent boundary layer separation [4].

Research into high speed plasma actuators have also been conducted [4, 5]. These types of flow actuators may be necessary components in future control implementations to successfully prevent unstart because of the fast propagation with which it can occur in certain settings.

Previous hypersonic experiments have shown that Wheeler doublets can be used to stabilize the flow in a ramjet isolator model [6]. Furthermore, the Wheeler doublets were used in conjunction with vortex generator jets to achieve a simplified control implementation in which unstart could be prevented under certain circumstances with a 50% success rate.

Closed-loop shock control experiments have also been previously carried out using back pressure flaps. Hutzel first tested six methods of determining the location of the leading edge of a shock train using tunnel-mounted pressure transducers [7]. As a result of these tests, a "pressure rise method" was selected

for further use and implementation [8]. Dynamic models were then developed using system identification techniques to describe the shock train leading edge dynamics [9]. These models were subsequently used to implement and validate a control scheme that could place the leading edge of the shock train in a $\pm 50\%$ duct height range about the desired location using a back pressure ramp with a 10 Hz bandwidth.

To aid in the control of the shock structure, research has been conducted into the process of performing system identification on the dynamics of the shock structure within the isolator [10]. System identification was performed on two distinct experimental facilities using the Hammerstein-Weiner model as the structure for the dynamics. The first experimental facility utilized was a direct-connect supersonic combustion facility at the Air Force Research Laboratory (AFRL) that simulated Mach 5 flight conditions. Tests were conducted with both rectangular and circular flowpath geometries. The second facility utilized was a blow-down supersonic wind tunnel located in the Flowfield Imaging Laboratory at the UT Austin Pickle Research Campus (PRC). This facility used an inlet/isolator model placed into a Mach 5 flow to replicate freestream flight conditions. The Hammerstein-Weiner model that was utilized for the system identification is a nonlinear dynamic model that assumes a linear base structure, but places nonlinearities on both the input and output signals. A simplified version of this model was also investigated [10].

One main distinction between the shock control research conducted by Hutzel [7] and the research detailed here is the specific algorithm utilized for shock detection. Hutzel tested several schemes to detect the leading edge of

an oblique shock train. In this research, a previously developed shock localization scheme is implemented that utilizes a Kalman filter based fusion of two different shock detection algorithms to determine the position of a normal shock within the isolator [11]. This method allows for a robust and accurate estimation of the shock position, and it is modular which allows other shock detection algorithms to be integrated. This implementation of the Kalman filter based localization scheme will be described in more detail in Section 4.1.

## 1.4 Research Contributions

The research detailed in this thesis addresses the challenge of preventing inlet unstart through closed-loop control of shock location in the isolator. This is accomplished through the experimental implementation of a shock localization scheme that utilizes a Kalman filter based fusion of two distinct shock detection algorithms. This shock position information is then utilized as feedback for various closed-loop control schemes in a Mach 1.8 direct-connect wind tunnel using a motorized back pressure flap as the primary means of actuation. This research also aims to identify important system parameters that should be considered during the design and implementation of closed-loop shock control [12].

In Chapter 2, the experimental facilities used in this research are described in detail. Chapter 3 describes the experimental setup used for the development and validation of various closed-loop shock control schemes. In Chapter 4, a detailed description is given of the various components of the closed-loop shock control system including the shock detection algorithms,

methods of shock actuation, and the different types of control logic that were implemented. The performance of each closed-loop controller is discussed as determined through experimental tests.

# Chapter 2

# Experimental Facilities

An experimental facility was constructed at the University of Texas at Austin Pickle Research Campus (PRC) to perform research into closed-loop shock control. A Mach 1.8 supersonic wind tunnel was designed and fabricated specifically for this purpose as shown in Figure 2.1. The wind tunnel consists of a convergent-divergent nozzle which is directly connected to a test section with transparent sidewalls that imitates the isolator portion of a scramjet engine. The test section is 4" wide $\times$ 1.5" tall $\times$ 26.5" long. The transparent sidewalls allow Schlieren imaging to be recorded during experimental tests. The wind tunnel also contains a set of aluminum honeycomb wafers and perforated screens in the plenum that serve as flow conditioners.

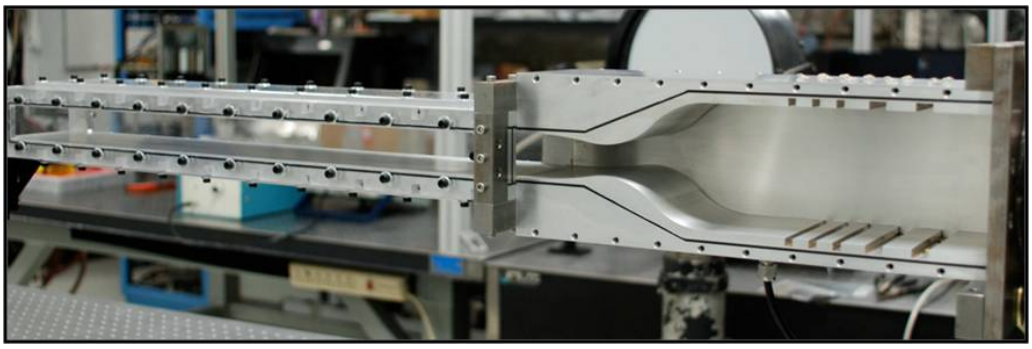

Figure 2.1: Mach 1.8 Direct Connect Wind Tunnel

The direct-connect wind tunnel was integrated into the existing high-

pressure facilities at PRC which utilize a Worthington Four-Stage Compressor to pressurize air into a group of eight storage tanks which are shown in Figures 2.2 and 2.3.

Figure 2.2: Worthington Compressor

Figure 2.3: High Pressure Storage Tanks

The air supply to the wind tunnel is controlled by a Sullivan & Sons, Inc. pneumatic positioner shown in Figure 2.4 which accepts a 3-15 psi air signal to regulate the position of the control valve. This signal is provided by a Fisher 846 I/P transducer which converts a 35 psi air supply into a 3-15 psi varying air signal based upon a commanded 4-20 mA current signal.

Figure 2.4: Sullivan & Sons Pneumatic Positioner

A LabVIEW Virtual Instrument (VI) software program was created to produce the necessary 4-20 mA signal for the I/P transducer using a National Instruments CompactRIO chassis and the NI 9265 output module. This module has 4 analog outputs that can produce a 0-20 mA signal at 100 kilosamples per second (kS/s). The LabVIEW VI developed to control the airflow to the wind tunnel allows for two modes of operation. The electrical control signal can be manually manipulated through a slider that directly controls the cur-

rent output or alternatively, the wind tunnel can be automatically controlled via a proportional-integral (PI) controller that outputs the necessary current signal to achieve the desired stagnation pressure as measured in the plenum of the wind tunnel. The stagnation pressure of the wind tunnel is measured by a Setra Model 204 absolute pressure transducer which is capable of measuring 0-100 psia pressures. This transducer outputs a 0-5 V signal based upon the measured pressure. The transducer voltage signal is sampled using another module installed in the CompactRIO chassis. The NI 9215 module is capable of 16-bit simultaneous sampling of 4 analog inputs. This card was utilized to sample the Setra pressure transducer output voltage and transfer the data into the LabVIEW VI. The CompactRIO and installed modules are shown in Figure 2.5,and the front panel of the wind tunnel control terminal is displayed in Figure 2.6.

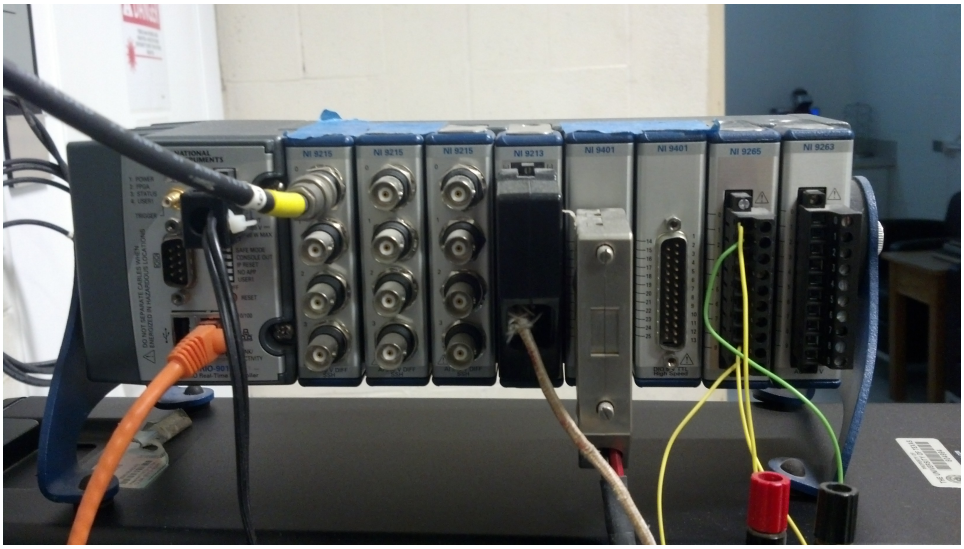


Figure 2.5: CompactRIO Chassis with Installed Modules

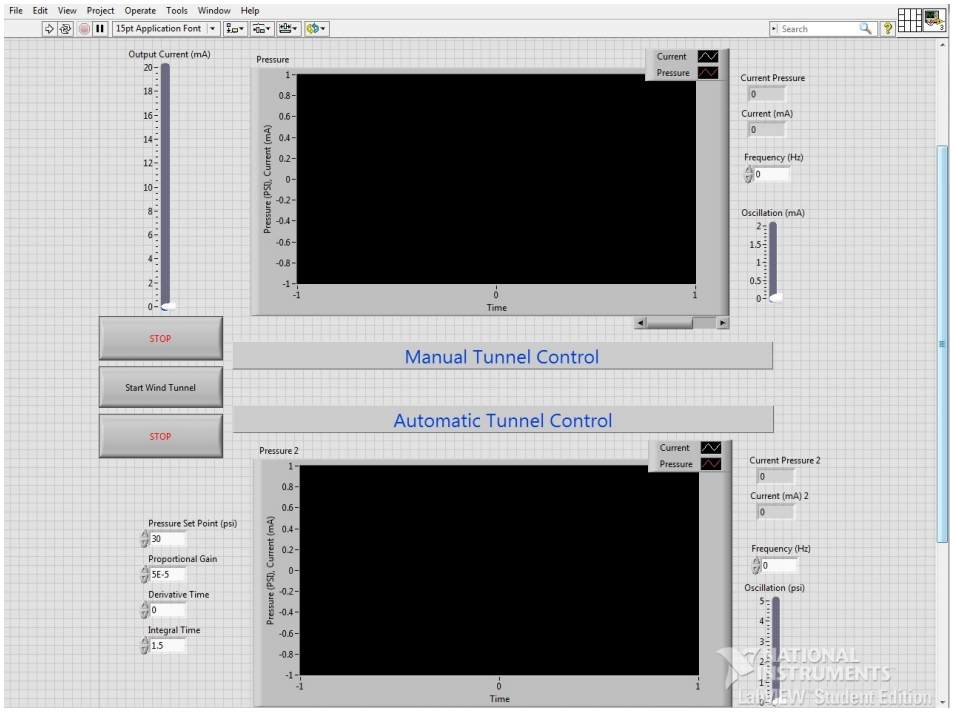


Figure 2.6: Front Panel of Wind Tunnel Control VI

# Chapter 3

# Experimental Setup

## 3.1 Pressure Acquisition

The first portion of the experimental setup consisted of instrumenting the wind tunnel test section with pressure transducers. Seven Kulite high frequency pressure transducers were installed in the ceiling of the test section at the locations shown in Figure 3.1. These allow static pressure measurements to be recorded along the length of the tunnel which are required for the real-time implementation of most shock detection schemes. One transducer was placed at the foremost part of the tunnel. Five transducers were placed with one inch spacings to create a high density region of transducers. The seventh transducer was placed as far aft as possible in the isolator while remaining within the length constraint imposed by the calibration cavity which is described in more detail shortly. This setup allows for accurate shock position estimation in the high density region while also allowing for a large range of shock detection throughout the majority of the isolator. This setup also allows for testing of the shock localization algorithm as the shock moves between the high and low density regions. A combination of two different models of Kulite transducers were used during shock control experiments which are the XCQ-062-15A and XCQ-062-50A models. These transducers have an absolute

pressure measurement range of 0-15 psia and 0-50 psia respectively.

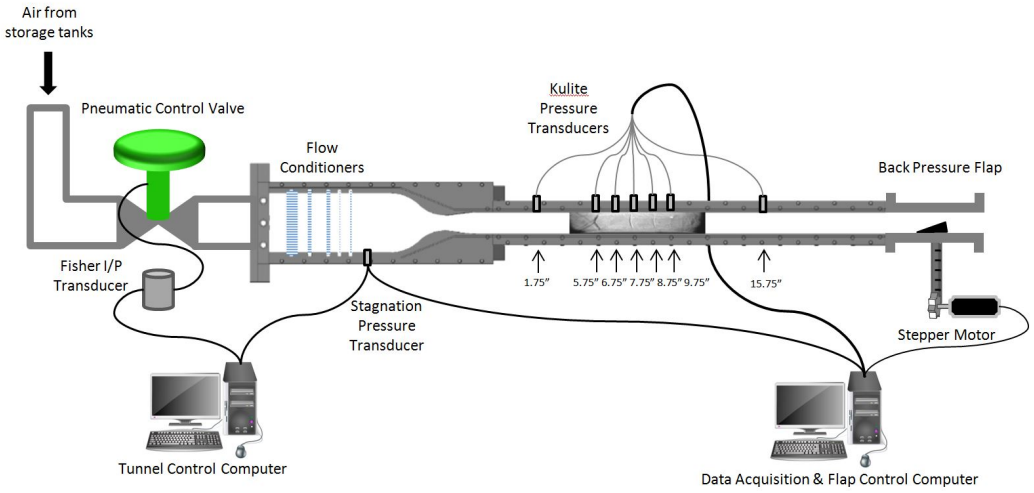


Figure 3.1: Mach 1.8 Wind Tunnel Schematic

The Kulite transducers require electrical excitation to produce a signal which then needs to be amplified prior to measurement. Both the excitation and amplification are accomplished through the use of Dynamics electrical amplifiers with adjustable gains shown in Figure 3.2.

The gains were adjusted to ensure that a 0-15 psia pressure measurement would output a voltage between -10 V and +10 V which is the measurement range of the NI USB-6356 DAQ card. The amplified pressure signals are then sent through a set of DL Instruments Model 4302 analog electrical filters shown in Figure 3.3. These filters are set to low-pass filter the pressure signals with a cutoff frequency of 2 kHz. The filtered signals are then sampled by a National Instruments X-Series USB-6356 Data Acquisition (DAQ) Board shown in Figure 3.4 which is connected to an Emachines personal computer via a USB connection. The USB-6356 is a multifunction DAQ board that


Figure 3.2: Electrical Amplifiers for Kulite Transducers

allows the user to simultaneously sample 8 analog inputs at speeds up to 1.25 megasamples per second. It also has two analog outputs and 24 digital I/O lines that can be utilized.

Figure 3.3: Analog Filters


Figure 3.4: NI USB-6356 X-series Multifunction DAQ Device

The Kulite pressure transducers must be calibrated before they can be utilized to make pressure measurements. To accomplish this, the transducers were installed in the removable ceiling of the wind tunnel test section. A rectangular aluminum pressure cavity was carefully sealed onto the inner surface of the ceiling ensuring that all transducers were completely inside the cavity. An Edwards vacuum pump and Setra Model 204 absolute pressure gage were connected to the cavity as shown in Figures 3.5 and 3.6. Pressure measurements were then recorded while the pressure inside the cavity was modulated through the opening and closing of a valve. A LabVIEW Virtual Instrument (VI) was developed to allow the voltages from the Kulite transducers to be recorded simultaneously with the output voltage of the Setra transducer. A screenshot of the front panel of this VI after collecting data from a calibration run is shown in Figure 3.7. Analysis of the calibration data yielded a set

of coefficients that were programmed into the LabVIEW pressure acquisition and control software to allow the recorded voltages from the transducers to be converted to static pressures.


Figure 3.5: Edwards Vacuum Pump

## 3.2 Motorized Flap Installation

Another aspect of the experimental setup involved tunnel modifications, fabrication, and installation of a motorized flap into the wind tunnel to actuate the shock's position. A separate wind tunnel section was designed and machined for this purpose. This section was installed aft of the isolator


Figure 3.6: Kulite Pressure Transducer Calibration

to allow the flap's motion to affect the back pressure of the shock system.

The flap is geared through a rack and pinion gear set to a Kollmorgen NEMA 23 electric stepper motor which has a holding torque of 280 oz-in. The stepper motor also has a quadrature encoder mounted to the shaft that gives angular position feedback to increase motor positioning accuracy. The motor and gearing setup are shown in Figure 3.8.

The stepper motor is powered by a 2.5 Amp AC stepper drive which interfaces to a National Instruments UMI-7772 Universal Motion Interface shown in Figure 3.9. This board allows the stepper drive and encoder to in-

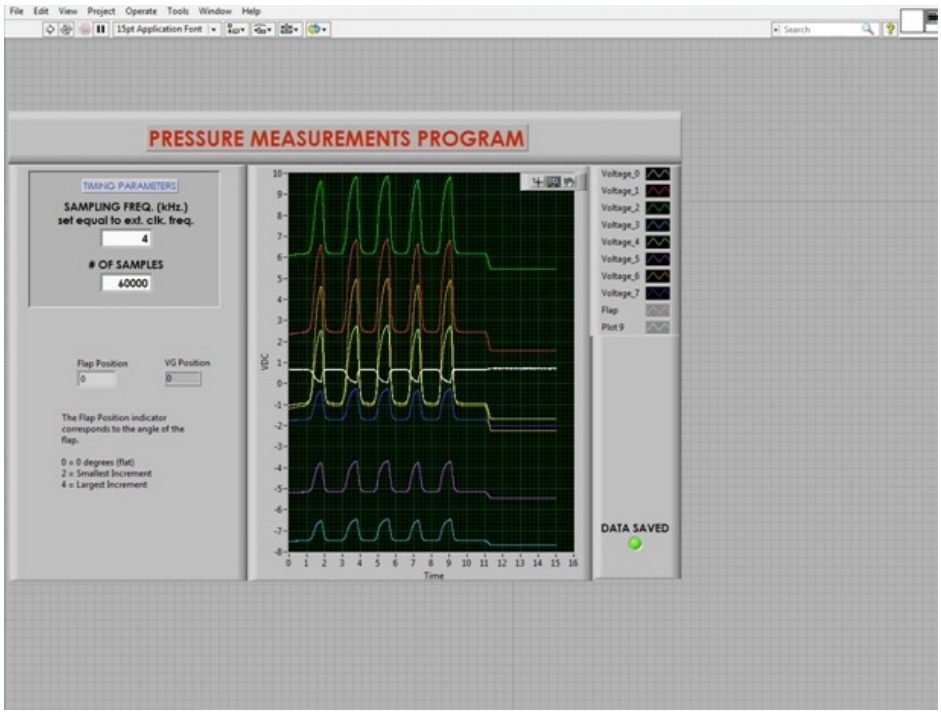


Figure 3.7: Pressure Measurements VI used for Transducer Calibration

terface with National Instruments PCI-7332 Stepper Motion Controller which is installed in an Emachines personal computer running LabVIEW 2012 software. The stepper drive was configured for use with the Kollmorgen stepper motor which has a command resolution of 5000 steps per revolution.

## 3.3 Schlieren Imaging Setup

A Schlieren imaging system was installed to allow clear video recording of the shock structure during experimental tests. The imaging setup consists of a ISSI Tri-Color LED Module that is driven by a Berkeley Nucleonics Corp (BNC) Model 500 pulse generator which are shown in Figures 3.10 and 3.11

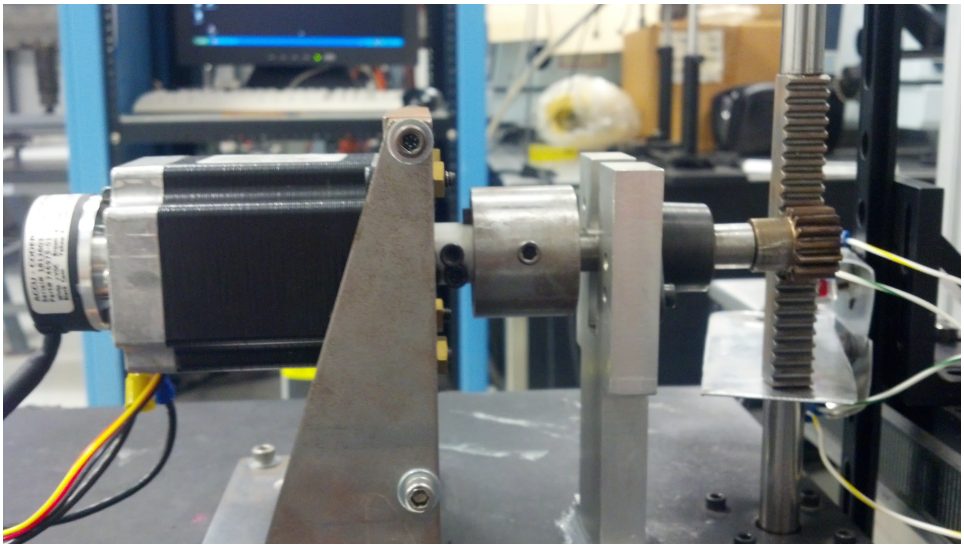

Figure 3.8: Stepper Motor and Gearing Setup

respectively.

The LED is aimed at the center of a 1 foot diameter, f/6, concave mirror shown in Figure 3.12 which is 1 focal length away from the light source. The collimated beam passes through the transparent sidewalls of the wind tunnel and onto an identical concave mirror which focuses the light back into a point after reflecting off of a flat mirror. A knife edge is then inserted into the focused point of light to create the Schlieren effect. The Schlieren images are captured by a Photron FastCam Ultima APX high-speed camera. The Photron high-speed camera settings were adjusted to capture only the test section in the field of view by recording at a 1024 x 128 image resolution. During initial tests, the camera was operated at 2000 fps to validate the shock localization techniques. However, a frame rate of 125 fps was found to be sufficiently fast for the majority of the closed-loop control tests that followed. This setting


Figure 3.9: NI UMI-7772

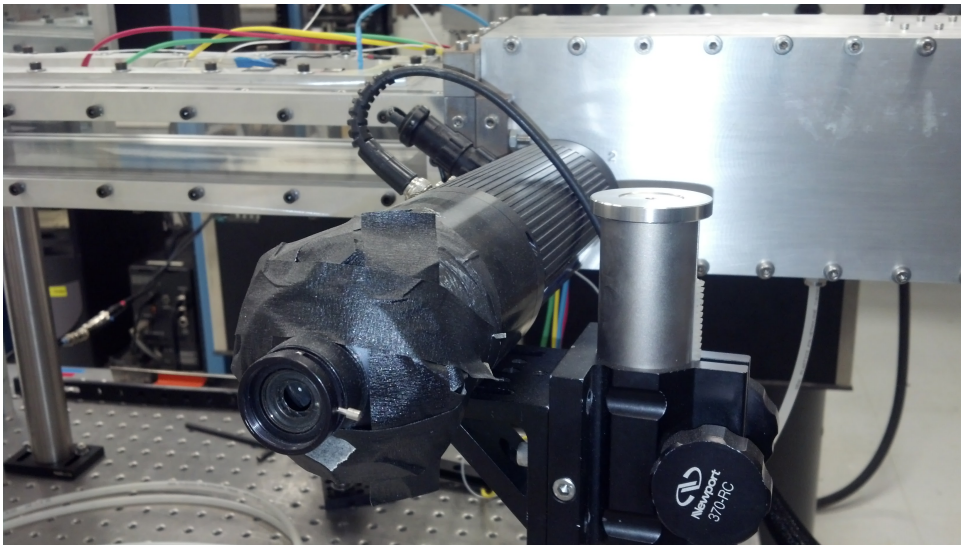


Figure 3.10: ISSI Tri-Color LED

was utilized to decrease the file size of each Schlieren video. The Photron Ultima APX also has the capability to output a step voltage signal when image recording begins followed by another step signal when recording terminates.

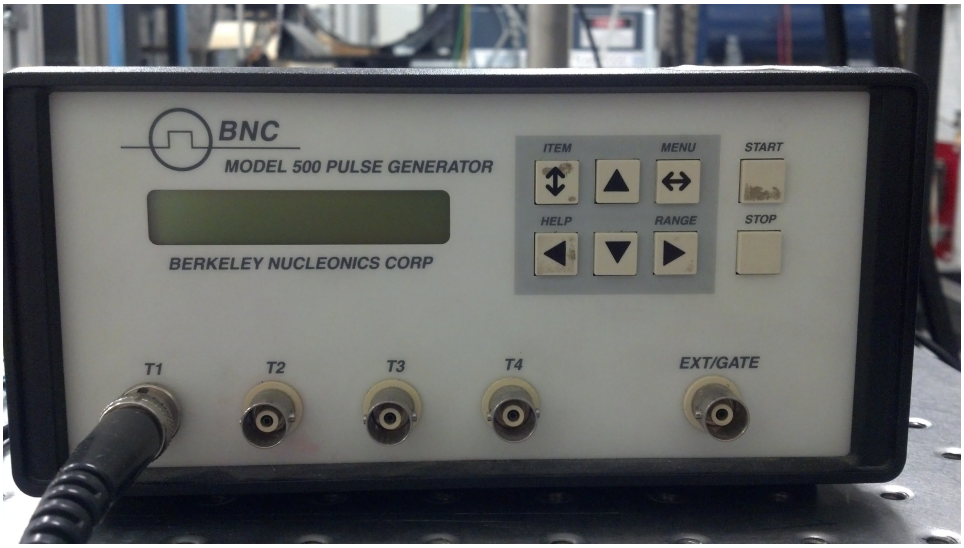


Figure 3.11: BNC Model 500 Pulse Generator

This capability allows for the acquired pressure data to be synced with the Schlieren images during post-processing. This allows for optical validation of any shock localization schemes tested with this system.

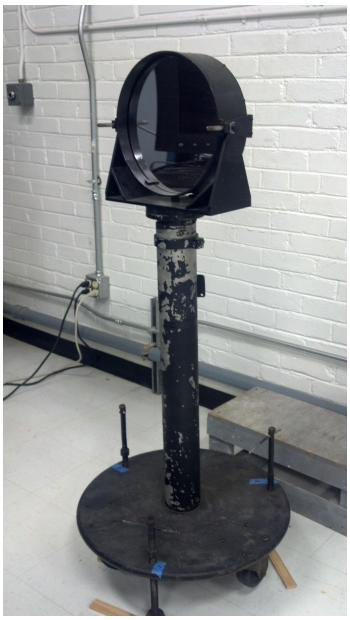

Figure 3.12: Concave Mirror

# Chapter 4

# Controller Design and Implementation

Closed-loop control of the shock location fundamentally requires implementation of three distinct concepts - sensing, actuation, and control logic. The following sections will detail how each of these concepts were implemented for experimental purposes. LabVIEW 2012 software was utilized to develop and execute all aspects of the tested control schemes [13]. LabVIEW is a graphical development environment produced by National Instruments. It allows users the ability to write code graphically using pre-built function blocks that can be connected via "wires" to control the flow of information throughout the program. This software solution also allows for fast, easy interfacing with hardware devices such as data acquisition (DAQ) cards. LabVIEW was chosen for this implementation because of its ability to quickly integrate programmed control logic with National Instruments hardware such as DAQ devices and motion controllers.

## 4.1 Shock Localization

Sensing of shock location is a complex issue that has been extensively investigated by many others. Several algorithms have been developed to localize shock position based upon static pressure measurements made along the

length of the tunnel test section. Some algorithms are designed to detect the leading edge of an oblique shock train [14, 15] while others are intended for use in localizing the position of a terminal or normal shock [16, 17, 18, 19, 20]. The implementation that will be detailed here utilizes a novel Kalman filter based fusion of two distinct shock detection algorithms.

The first and primary algorithm that was utilized in the experiments is a geometrical shock detection algorithm [11]. This algorithm takes a pressure signal which consists of a set of static pressure measurements at known tunnel positions and fits a cubic spline through the $n$ data points. This cubic spline is then resampled at a higher resolution generating a curve with $m$ data points where $m > n$. An exponential curve is then fit through the $m$ resampled data points using the method of least squares. A difference signal is computed from the two curves as shown below:

$$\Delta(x) = P_{cub}(x) - P_{exp}(x) \tag{4.1}$$

The difference signal is then scanned from the aft most part of the isolator forward. A series of checks is used to find the position of the shock. The difference signal is always negative at the aft end of the isolator. A boolean variable is set to false when the scan initiates. As the scan progresses forward, the first index where the difference signal is positive, the boolean variable is set to true. The scan continues to progress forward. The next index where the difference signal becomes negative (while the boolean is set to true) triggers the algorithm to output the shock position as the last position before the

difference signal became negative. An example of this algorithm executing on a typical pressure profile is shown in Figure 4.1.

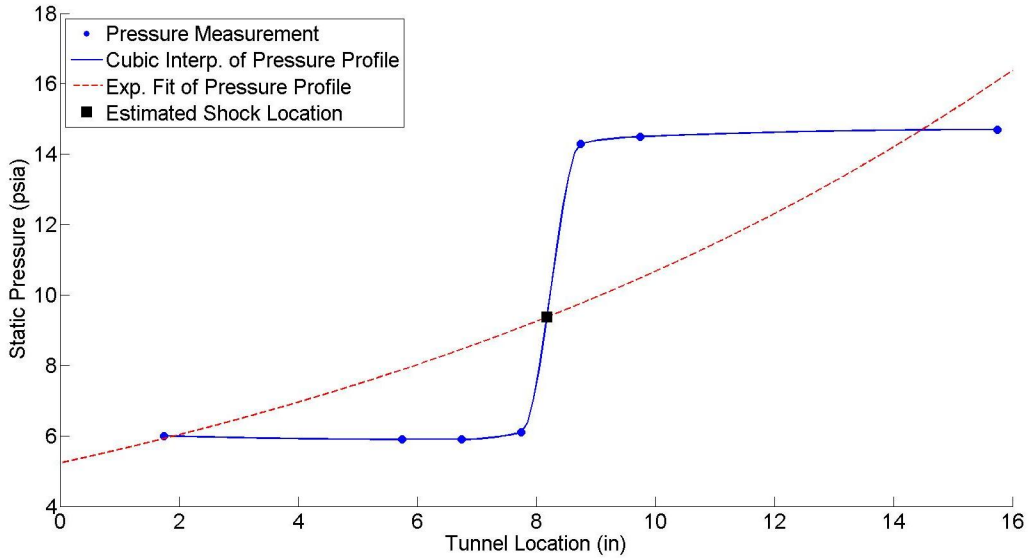


Figure 4.1: Geometrical Shock Detection Algorithm

Transducer spacing is a vital aspect of the shock sensing implementation. The distance between transducers can place a strict limitation on the resolution of the shock location estimate depending upon the chosen algorithm. As a result, the transducer spacing can be a limiting factor in the performance of a given shock control implementation. Experiments revealed that the transducers must be spaced closer together than the desired command resolution.

It is important to recognize that because of the sensitivity of the geometrical algorithm to transducer spacing, it is susceptible to inaccuracy in the event of a transducer failure. An example of this algorithm operating in the

event of a single transducer failure is shown in Figure 4.2. In this example, the failed pressure transducer is outputting an erroneous voltage corresponding to a 0 psia measurement. There are many possible failure modes for various pressure transducers, but this illustration demonstrates that the geometrical algorithm is susceptible to a single-point of failure. The failure of one transducer can have a significant effect on the interpolation and curve fitting processes such that the geometrical algorithm will return an erroneous estimate of the shock location.

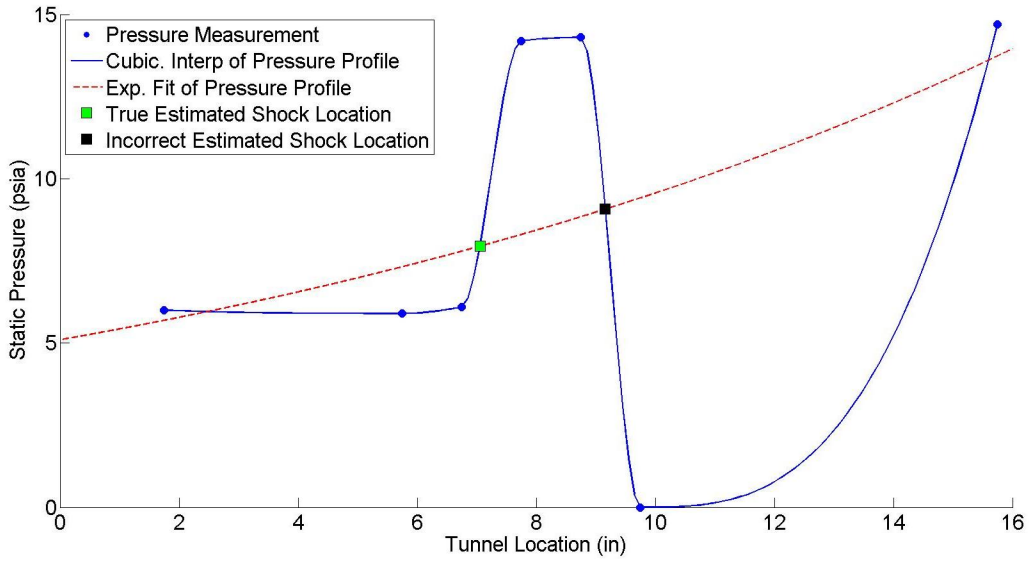


Figure 4.2: Geometrical Algorithm during Transducer Failure

As a result of this lack of robustness to transducer failure, the Kalman filter framework was implemented to fuse the estimate from the geometrical algorithm with an estimate from a summation-of-pressures algorithm. The sum-of-pressures (SOP) algorithm has been used in various implementations

for shock detection [19]. This algorithm estimates shock location through its correlation to the summation of static pressures throughout the isolator. Generally, experiments are conducted on a specific system to determine the relationship between the position of the shock and the sum of static pressures as measured throughout the isolator. The sum-of-pressures algorithm implemented here determines this relationship dynamically during execution instead of requiring a priori knowledge of the function. As the algorithm executes, the sum of static pressures at each instant is correlated to the shock position estimate as determined by the geometrical algorithm. A quadratic curve is assumed to fit the data set for this research, but higher order polynomials can be used. The coefficients of the quadratic curve become states in the Kalman filter that are dynamically updated as the filter executes. A shock estimate can then be obtained by solving the quadratic polynomial using the most recent estimates for the quadratic coefficients and static pressure measurements. A typical sum-of-pressures profile and its corresponding quadratic fit is shown in Figure 4.3. With this scheme, the summation-of-pressures algorithm becomes tuned as the filter executes adding a level of robustness to the composite shock location estimate.

Estimates from both localization algorithms are weighted equally in the current software implementation, but the Kalman filter also allows for differential weighting among various estimates. In general, the sum-of-pressures algorithm is not as accurate as the geometry-based algorithm, but it is typically more robust to transducer failure. If a large number of transducers are utilized, the failure of one does not significantly affect the sum of static

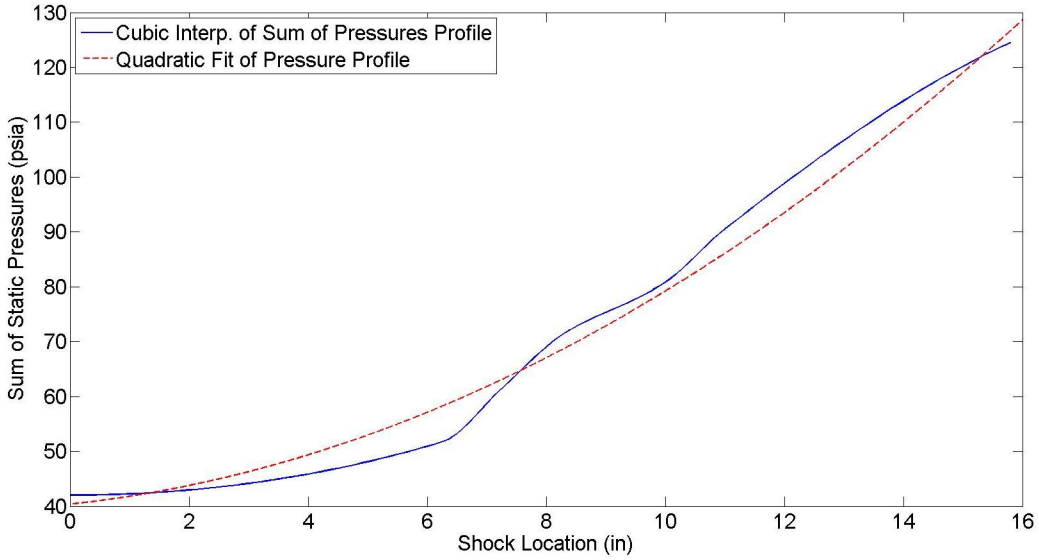


Figure 4.3: Sum of Pressures Algorithm

pressures. As a result, the sum-of-pressures method is not as heavily affected by transducer failure as the geometry-based method. If a failure is detected, the weight assigned to each algorithm's estimate could be adjusted to give more weight to the more robust SOP algorithm and thereby prevent the geometrical algorithm from erroneously driving the composite estimate in these circumstances.

Another crucial aspect in the experimental implementation of the shock localization scheme is the execution speed of the detection algorithm. The Kalman filter based shock localization algorithm was programmed in LabVIEW 2012 to allow for simple interfacing with National Instruments data acquisition devices [13]. In general, LabVIEW programs that run on personal computers are limited in execution speed by the task scheduling of the com-

puter's operating system and the computer's processing capabilities. Using a personal computer running Windows 7 with an Intel Pentium E2180 2.0 GHz dual-core CPU, a variable execution speed of approximately 33 Hz was initially attained when executing the shock localization software. This configuration was utilized for most control experiments. Modifications were subsequently made to the shock control software to change the data acquisition configuration from an on-demand sampling configuration to a fixed sampling rate using a buffer. Following this set of software modifications, the shock detection algorithm executed at a rate of 250 Hz.

## 4.2 Shock Actuation

Two methods of actuation for the shock structure were experimentally tested. The first actuation method utilized a motorized flap downstream of the isolator which could be raised and lowered to affect the back pressure of the isolator and thereby move the shock.

Initial closed-loop control experiments revealed that the actuator resolution was insufficient for our purposes. Commanding the smallest increment of motor movement yielded a large change in shock position which made it impossible to reach the desired set point in certain experiments. This revealed that higher resolution actuation would be required to finely control the position of the shock. To increase the actuation resolution a new gearing setup was purchased and installed. The original 10 pitch 1.2" diameter spur gear was replaced with a new 20 pitch 0.85" diameter spur gear and matching rack. This allowed a commanded angular rotation of the stepper motor to produce

a smaller corresponding change in flap angle.

The second actuation method attempted to utilize a set of vortex generators (VGs) similar to those shown in Figure 4.4 which were installed in the upstream portion of the isolator test section. These VGs could be oscillated into and out of the flow at various frequencies by an AGAC Derritron electromechanical shaker shown in Figure 4.5. This actuation was performed in an effort to energize the boundary layer, prevent separation, and move the shock downstream. Many tests were conducted on this form of actuation in the wind tunnel utilizing different vortex generator sizes and configurations and oscillating at various frequencies, but they never accomplished the desired result of moving the shock downstream. The only observed effect of the VGs on the flow was to serve as a blockage when raised thereby resulting in the slight upstream movement of the shock structure. As a result of these tests, the use of vortex generators as a viable shock actuation method for closed-loop control was not considered further in this particular study.

## 4.3 Control Schemes

The first control scheme that was implemented was a simple switching mode (i.e. logic-based) controller that compared the current shock position to the commanded position and then actuated the flap motor a constant number of steps in the appropriate direction to decrease the error. This type of control scheme is very easy to implement because of the simple logic, but experiments demonstrated that its performance in controlling the shock system was relatively poor.

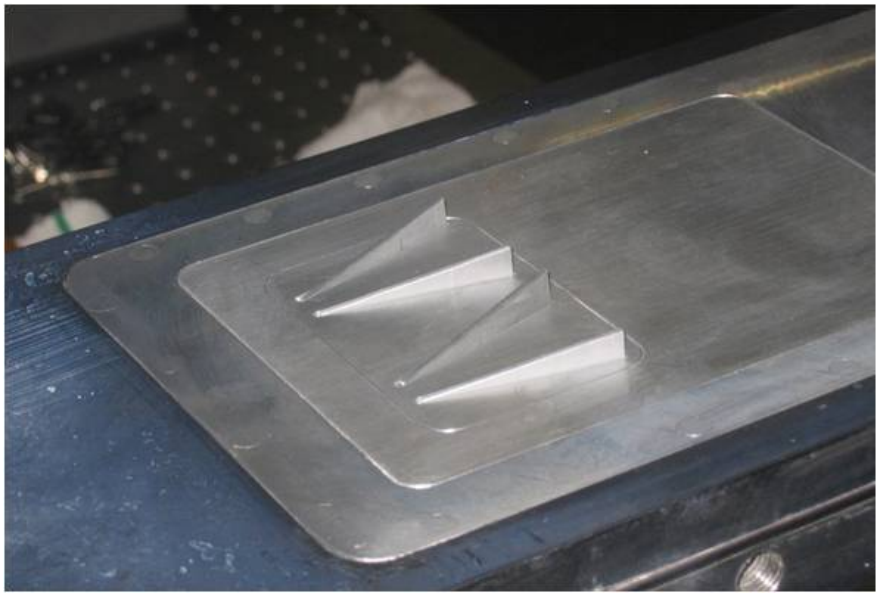

Figure 4.4: Vortex Generators

The second control scheme to be implemented was a proportional-derivative (PD) controller. This was accomplished using the integrated PID controller algorithm found in LabVIEW 2012 [13] which has native controls for simple gain tuning, output limiting, and other useful features. For this integrated PID controller, the control action is determined as detailed below [21].

At every iteration (k), the error is calculated as the difference between the set point (SP) and process variable (PV).

$$e(k) = SP - PV \tag{4.2}$$

The proportional control effort is calculated by multiplying the controller gain times the current value of the error as shown below:

$$u_P = K_c * e(k) \tag{4.3}$$

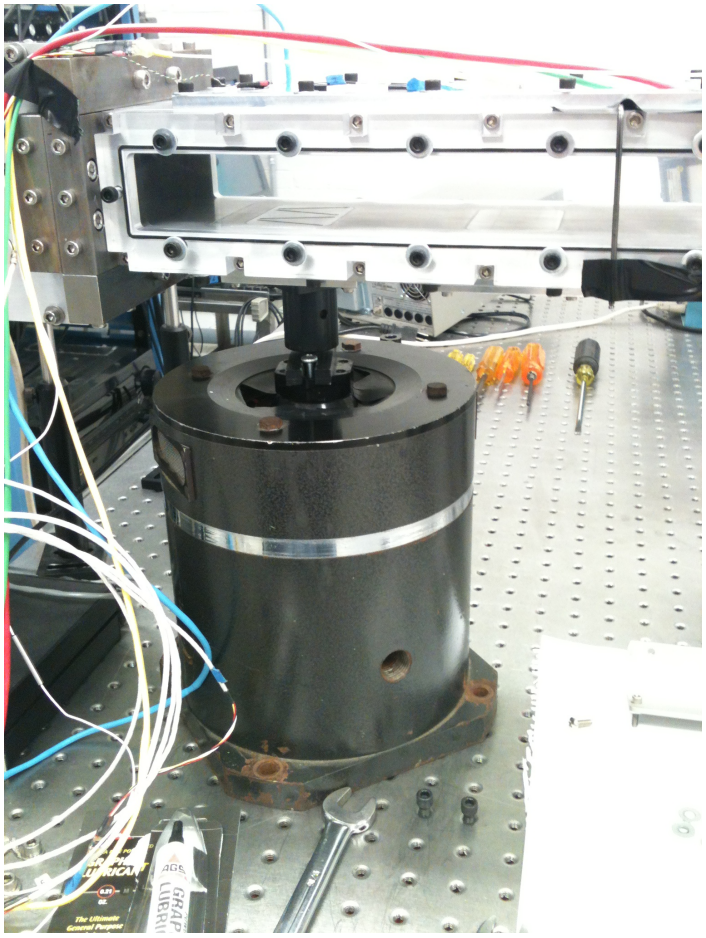

Figure 4.5: Electromechanical Shaker

The integral control effort is calculated using a trapezoidal integration method where $T_i$ is the integral time and $\Delta t$ is the time step size:

$$u_I = \frac{K_c}{T_i} \sum_{i=1}^{k} \left[ \frac{e(i) + e(i-1)}{2} \right] \Delta t \tag{4.4}$$

The derivative control action is calculated using only the process variable to prevent derivative kick from occurring when the set point is changed. The partial derivative control action utilizes a derivative time $T_d$ to calculate

the control effort as follows:

$$u_D = -K_c \frac{T_d}{\Delta t}(PV(k) - PV(k-1)) \tag{4.5}$$

The final control effort that is applied at every time step is the sum of all three control actions:

$$u(k) = u_P(k) + u_I(k) + u_D(k) \tag{4.6}$$

Since the stepper motor only accepts commands as an integer number of steps to move, the control effort that was output from the PID algorithm had to be rounded to the nearest integer before being sent as a command to the motor.

The front panel of the LabVIEW Virtual Instrument (VI) utilized during experimentation is shown in Figure 4.6. This program has two separate loops that execute simultaneously. The first loop executes as fast as the computer operating system allows. It performs the shock localization procedure by reading in voltage measurements from pressure transducers, applying calibration coefficients, executing the geometrical and sum-of-pressures shock detection algorithms, determining a final shock location estimate, and storing all relevant data in a matrix to be saved when program execution is complete. The second loop is the motor control loop. This loop reads in the desired shock position and compares it to the current shock position as determined by the localization scheme. It then performs the specified control logic and outputs the resulting commands to the stepper motor.

The front panel has several controls that allow the user to interface with the program during execution. The user can select which shock localization estimate is utilized in real time – the geometrical position or Kalman filter estimate. The user can also specify individual parameters similar to gains that are used by the internal PID control algorithm to determine the commands for the stepper motor. Unlike the shock localization loop which executes as fast as allowed by the operating system, the motor control loop has a specified period of execution that can be controlled from the front panel. Furthermore, this loop can be turned on and off at will to initiate or cease shock position control and motor actuation. When experimentation is complete, the operator can stop the pressure acquisition upon which the user will be prompted to save a text file containing all of the collected data from the run.

## 4.4 Controller Performance

The first control scheme that was implemented utilized a switching mode logic in which the motor would be actuated a fixed number of steps in the appropriate direction to decrease the error between the commanded and measured shock locations. For the initial experiments, the logic controller was tested using a five step fixed increment with a one second motor control loop period. During these runs, several performance deficiencies were observed. First, the controller demonstrated a slow response. Second, when the shock was in the neighborhood of the commanded position, it would oscillate about the set point, but it could not converge. This was a result of the fixed five step size increment.

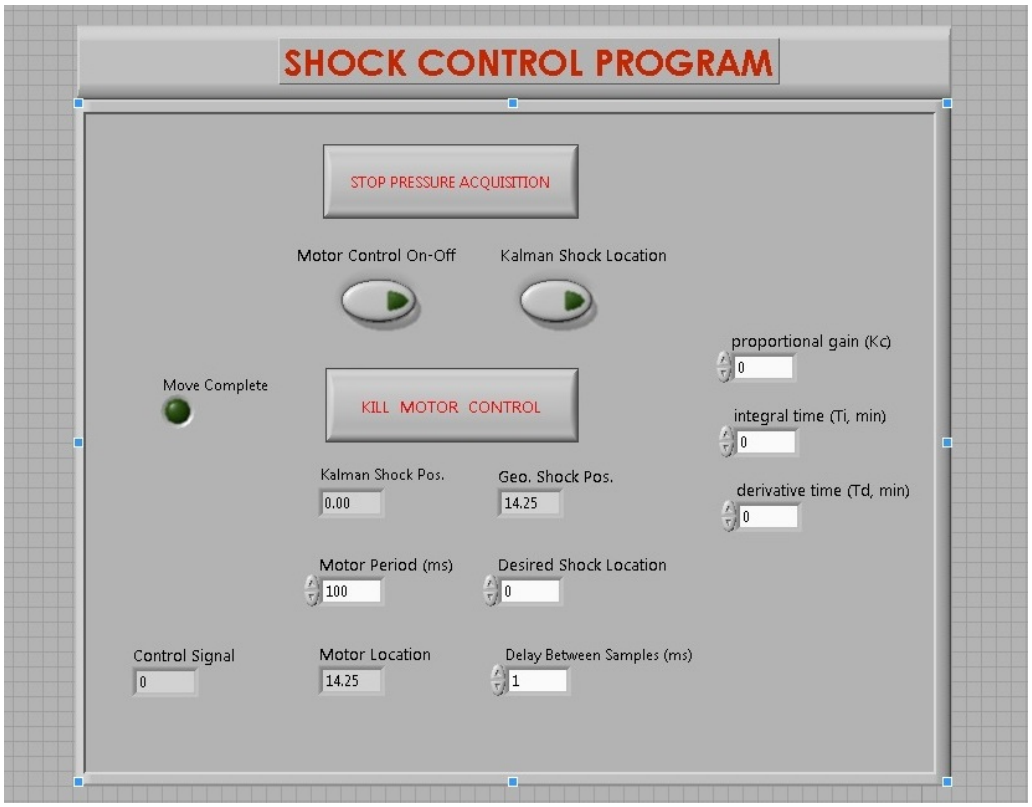


Figure 4.6: Front Panel of LabVIEW Shock Control Program

For the next set of experiments, the step size increment was reduced to a fixed four step increment to address the oscillations resulting from coarse actuation resolution. Furthermore, to address the slow response time, the motor control loop period was reduced from 1 second to 0.5 seconds and eventually to 0.275 seconds. A shorter period was not used to ensure that the actuation loop was executed approximately one order of magnitude slower than the 33 Hz shock localization loop. This was done to ensure that the controller acted upon recent shock position information. This new configuration yielded much better results. Two performance plots of this setup are shown in Figures

4.7 and 4.8. The top graph in each figure displays the desired and measured shock location during the experiment. The middle plot shows the position of the flap motor, and the bottom plot displays the tunnel stagnation pressure as measured in the plenum.

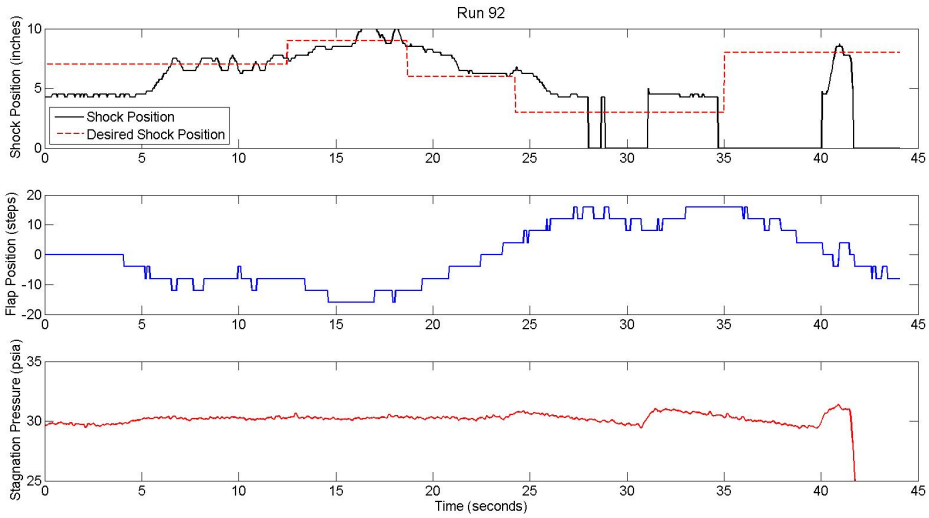


Figure 4.7: Switching Mode Controller Performance Plot

The top plots in each figure demonstrate that while the switching mode controller could force the shock toward the desired position, it still displayed many performance deficiencies, especially in controller response time. The controller was unable to consistently regulate the shock to the desired position even in the absence of stagnation pressure disturbances as shown in the bottom plot of Figure 4.8. Furthermore, the results shown in Figure 4.8 demonstrate how coarse transducer spacing can lead to control system failure. Whenever the shock moved forward of the 5.75" position into a coarse transducer region as shown in the top plot of Figure 4.8, the estimate of the shock position be-

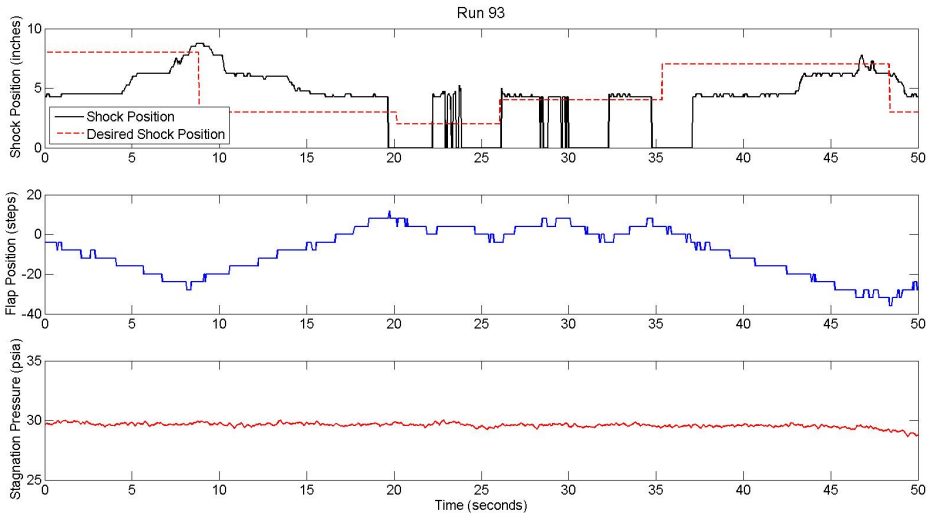


Figure 4.8: Switching Mode Controller Performance Plot

came very erroneous which led to incorrect command signals. This resulted in the high frequency switching nature of the measured shock location in the top plot and the inability of the controller to regulate the shock to a desired position forward of the 5.75" transducer. This deficiency demonstrates the importance of transducer spacing in determining shock location and subsequently controlling the shock position.

Although the switching mode controller was tested several times with various step sizes and motor control periods, satisfactory performance could not be achieved as the shock failed to converge to the commanded value. These tests did reveal a fundamental flaw in the setup. Even with one step increments, the shock would oscillate about the set point demonstrating that the actuation resolution was insufficient to drive the shock to the desired position. This necessitated a change in the gearing setup that was being utilized. To

address this issue, the rack and pinion gearset was replaced with a smaller diameter set as detailed in Section 4.2.

Following the switching mode controller, a proportional-integral (PI) controller was developed and tested. After conducting several experiments to tune the proportional and integral gains, the proportional-integral controller performed much better than the switching mode controller since it could adjust its command output based upon the current position error of the shock system. Unfortunately, this controller was unable to cause the shock system to completely converge to the desired location, but instead caused the shock to oscillate in a small range around the set point as shown by the top plots in Figures 4.9 and 4.10.

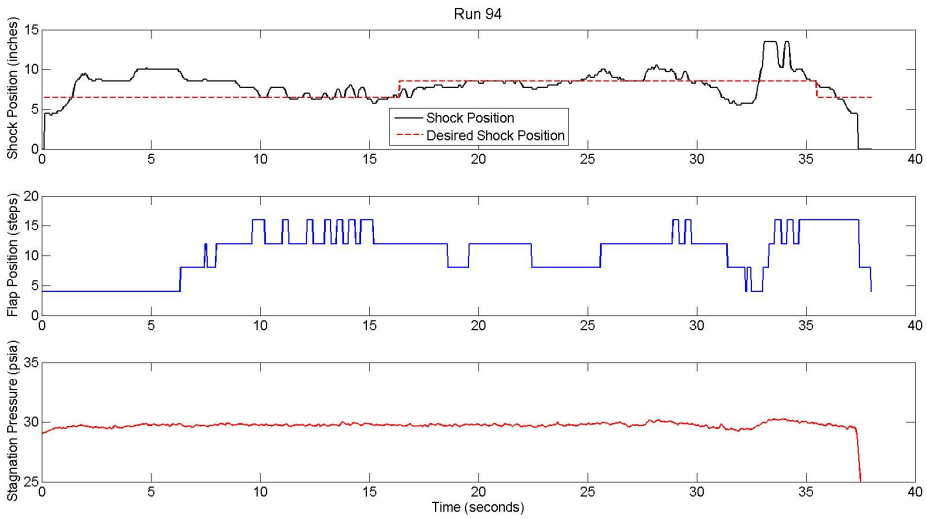


Figure 4.9: PI Controller Performance Plot ($K_P$=1, $K_I$=1.667)

It is important to note that the performance of the controllers tested depended heavily upon the size of initial oscillations. If an initial oscillation

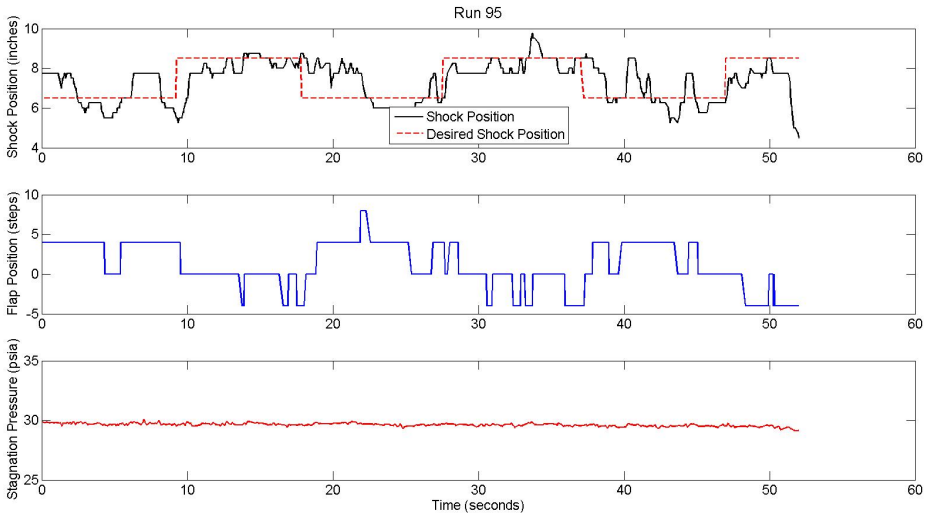


Figure 4.10: PI Controller Performance Plot ($K_P$=0.75, $K_I$=1.25)

was large enough to push the shock outside the region of dense transducer spacing into a region of course spacing, the shock estimate would deviate from the actual location and thereby induce a control response magnitude that was inconsistent with its actual location. When oscillations continually drove the shock into and out of the region of dense transducer spacing, regulation could not be achieved. This demonstrates the importance of transducer spacing not only in determining an accurate shock estimate, but also in calculating the appropriate control response. A sufficiently fine transducer spacing is vital to the success of this closed-loop control implementation.

After this set of experiments, the command mode of the motor was modified to increase controller performance. The motor can receive absolute or relative position commands. Absolute commands will send the motor to a certain position while relative commands move the motor a certain number

of steps from its current position. In absolute mode, the proportional term sent the motor to a certain position, and the integral term would reduce the error as time progressed. The motor mode was switched to operate in relative position mode so that a proportional term would prescribe a certain movement amount each iteration instead of a certain position.

As a result of the change in operational mode, a new set of tuning experiments had to be conducted. A proportional controller was first tested to find a suitable proportional gain before adding other terms. After tuning, an experiment using $K_P = 5$ was found to demonstrate some promising performance characteristics such as bounded oscillations within a small area about the set point as shown in Figure 4.11. This figure also demonstrates a deficiency of the controller in that even in the absence of stagnation pressure disturbances as displayed in the bottom plot, sustained oscillations were caused by the commanded flap position shown in the middle plot.

A derivative term was subsequently added into the control logic. Further tuning experiments were conducted to determine the appropriate gains. Two experimental runs demonstrated increased performance. The time response plots and corresponding gains are shown in Figures 4.12 and 4.13.

As the top plots of these figures show, the PD controller performed better than any of the previous control schemes in maintaining the position of the shock in a small region about the desired set point of 8" which lies inside the dense transducer region.

Although this controller demonstrated improved performance, the pe-

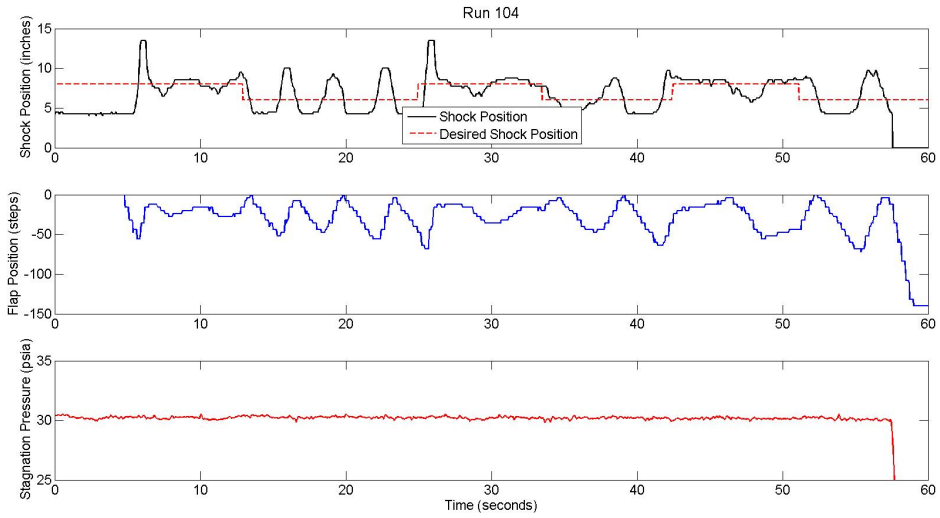


Figure 4.11: Proportional Controller Performance Plot ($K_P$=5)

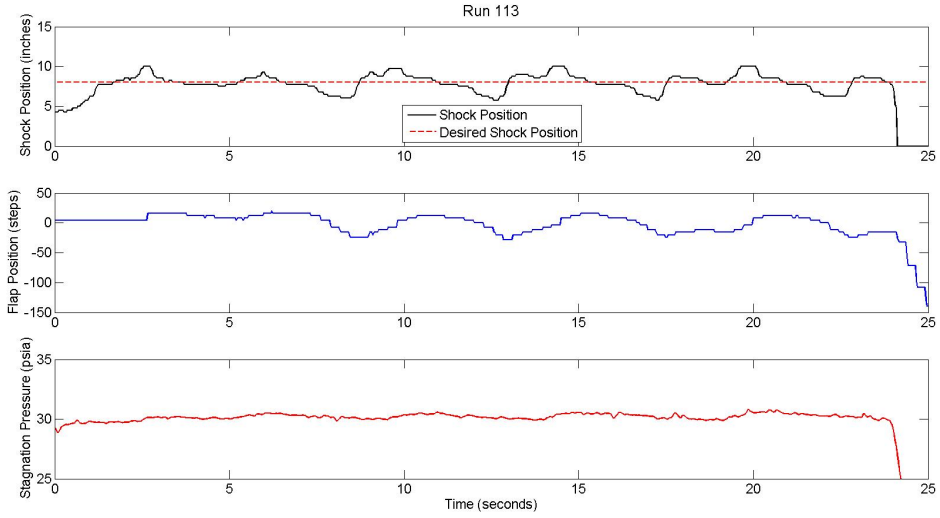


Figure 4.12: PD Controller Performance Plot ($K_P$=6, $K_D$=0.072)

riod of the motor control loop was further reduced to increase the response speed of the system. Various periods were tested, and 100 ms period was selected as it allowed the motor to still complete commands in the allotted time

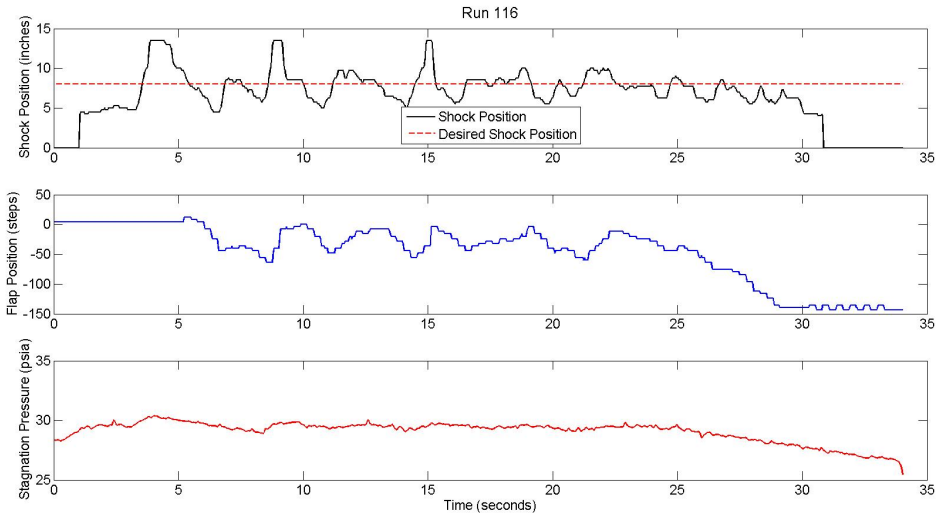


Figure 4.13: PD Controller Performance Plot ($K_P$=7, $K_D$=0.21)

between loops.

As a result of the change in execution period, more tuning experiments were conducted. A successful experimental run achieving regulation of the shock to the desired position was accomplished as shown in Figure 4.14. As the plot shows, the shock converged quickly to the 8" set point and remained there. The controller oscillated about the subsequently commanded 6" set point because the oscillations forced the shock forward of the 5.75" transducer which is outside of the dense transducer region represented by the green shaded area on the top plot. As a result, the shock position estimate lost accuracy which lead to inconsistent motor commands as can be seen in the middle plot of flap position commands. Small commands were given when the shock converged to the 8" position, but large commands were given around the 6" position because of the inaccurate position estimate leading to sus-

tained bounded oscillations about the desired set point. When the set point was returned to the 8" position, the controller quickly regulated the shock to the desired position. The results of this experiment once again reinforce the importance of transducer spacing in determining an accurate shock location estimate.

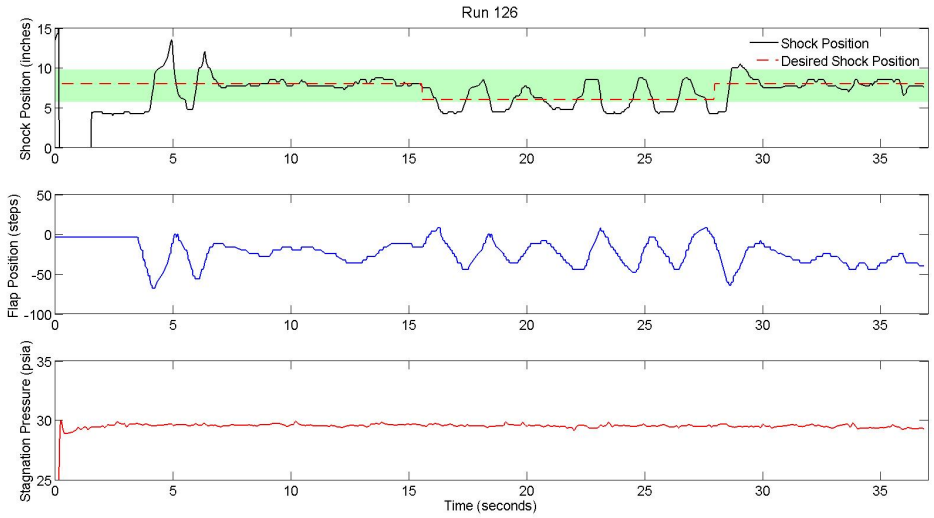


Figure 4.14: PD Controller Performance Plot ($K_P$=3.5, $K_D$=0.084)

After finding a set of control gains that yielded satisfactory regulation of shock position from an initial location to a final commanded position, the next set of experiments was conducted with the primary aim of testing the response of the controller to stagnation pressure disturbances of various magnitudes. The response of the system when subjected to a 0.2 Hz, 1 psia amplitude sinusoidal disturbance in stagnation pressure is shown in the bottom plot of Figure 4.15. As the top plot shows, the disturbances forced the shock out of the dense transducer region and effectively out of the test section by passing

the last transducer. The controller was unable to compensate for such a large, fast disturbance in stagnation pressure.

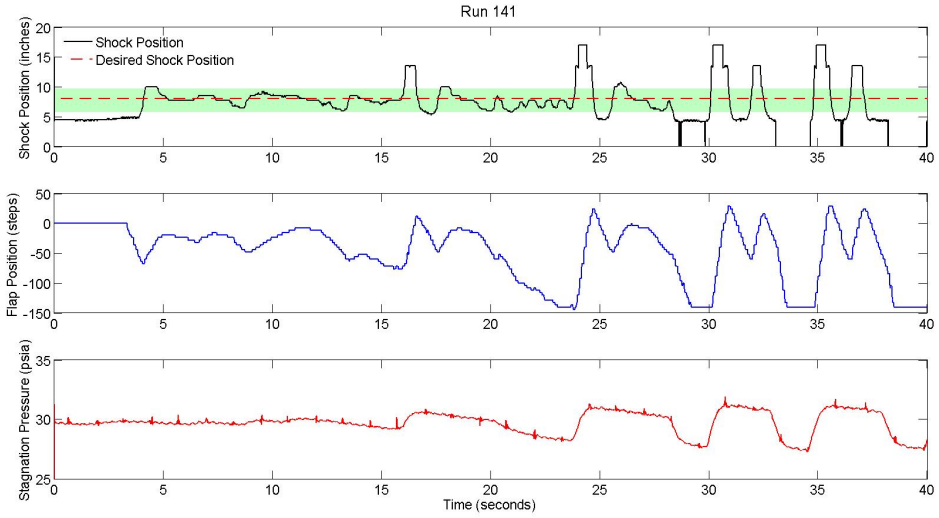


Figure 4.15: PD Controller Performance Plot ($K_P$=3.5, $K_D$=0.084)

As a result of this shortcoming, another experiment was conducted using a 0.2 Hz, 0.5 psia amplitude sinusoidal disturbance in stagnation pressure. The result of this test is shown in Figure 4.16. When subjected to a smaller disturbance of the same frequency, the controller was able to maintain the position of the shock inside the isolator. The shock did exit the dense transducer region, but the PD controller did not allow the shock to completely exit the monitored region of the test section. Higher frequency disturbances should also be tested, but 0.2 Hz oscillations seemed to be near the upper limit of the response time of the wind tunnel control valve. With faster tunnel control hardware, further tests could be conducted to determine the performance of the PD control scheme when subjected to high frequency disturbances.

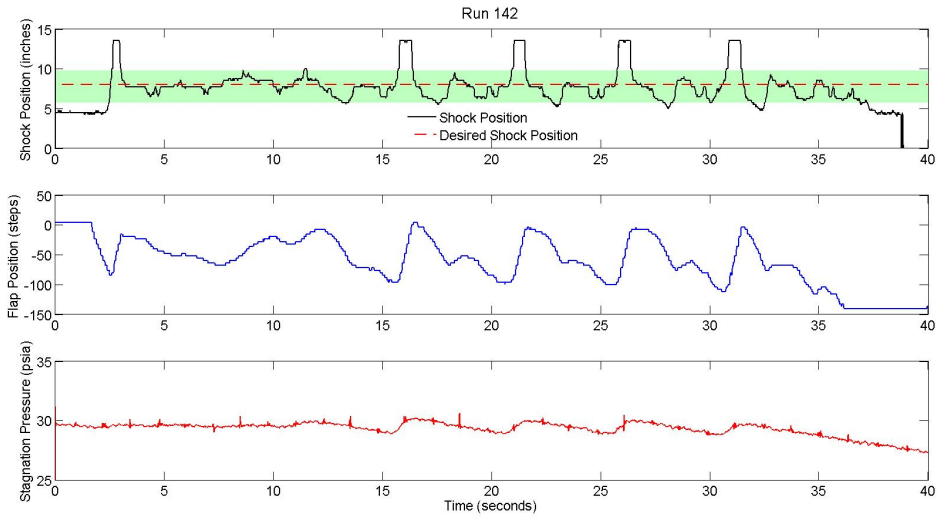


Figure 4.16: PD Controller Performance Plot ($K_P$=3.5, $K_D$=0.084)

The next set of experiments was conducted to investigate the performance of the controller in different operational regimes. The previous tests demonstrated the performance of the PD controller at regulating shock position in a dense transducer region in a certain portion of the isolator. The primary goal of this test was to investigate how this performance may vary if the dense transducer region and desired set point lie somewhere else inside the isolator. To perform this test, the dense transducer region was relocated 5" aft as shown in Figure 4.17.

In a similar fashion to the previous two disturbance tests, two more tests were conducted by subjecting the same PD control law to small and large disturbances while it attempts to regulate the shock position to a set point inside the relocated dense transducer region. The results of the large and small disturbance cases are shown in Figures 4.18 and 4.19 respectively. As the plots

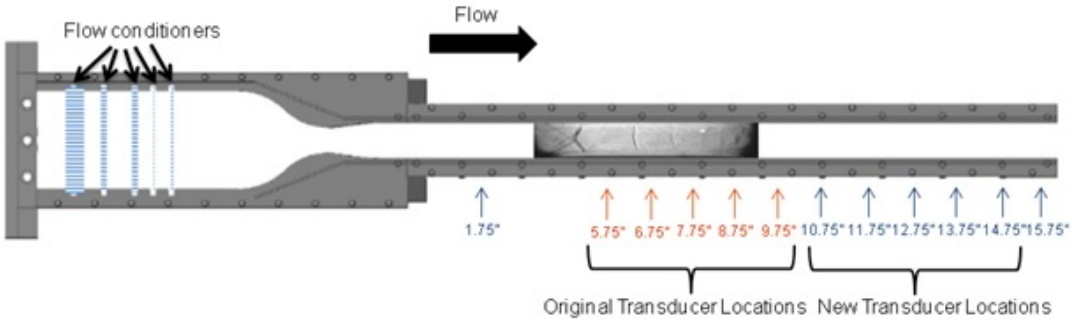


Figure 4.17: Modified Kulite Pressure Transducer Locations

demonstrate, a similar behavior is seen where the large disturbance causes the shock to move past the last transducer whereas the smaller disturbances are more easily regulated to remain within the dense transducer region. An interesting artifact appears on these plots which can be seen whenever the shock passes in front of the forward transducer in the dense transducer region at the 10.75" position. Since the dense region was relocated, there is now a 9" gap between the first and second transducers instead of a 4" gap. This leads to a much less accurate shock estimate when the shock resides in this coarse region. This rapid breakdown of the shock location estimate whenever it passes in front of the 10.75" transducer leads to the high frequency switching behavior that can be seen in the plots of shock location. As previously mentioned, this reinforces the important role transducer spacing plays in the performance of the closed loop system.

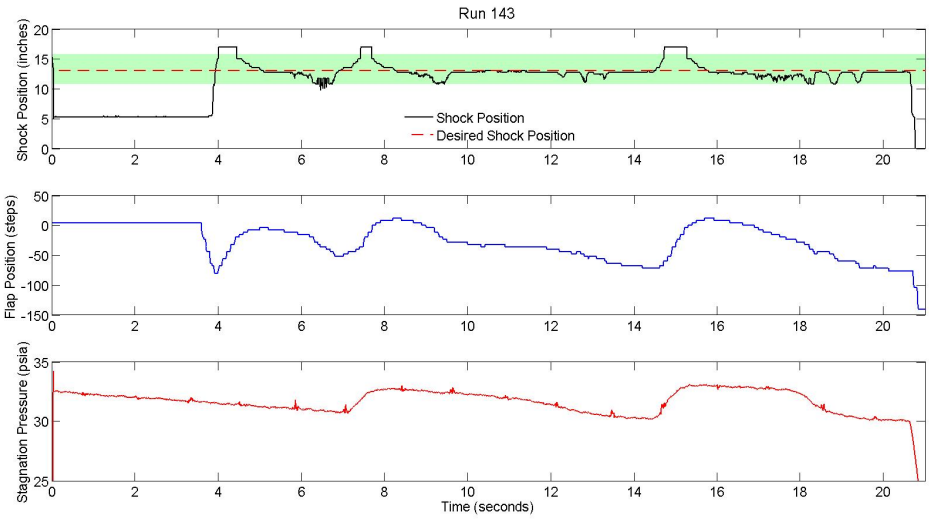


Figure 4.18: PD Controller Performance in Relocated DTR

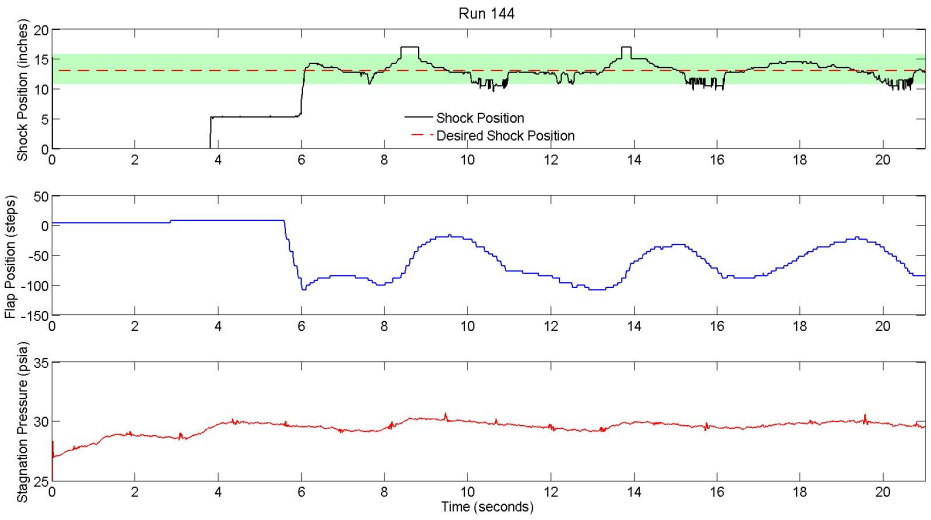


Figure 4.19: PD Controller Performance in Relocated DTR

# Chapter 5

# Conclusion

This research has demonstrated the real-time implementation of a Kalman filter based shock localization scheme which can accurately and robustly determine the position of a normal shock within an isolator by fusing the estimates of distinct localization algorithms operating on static pressure measurements. Furthermore, regulation of the shock's position has been experimentally demonstrated in the presence of mild upstream pressure disturbances through the use of a proportional-derivative controller actuating a motorized back pressure flap in a Mach 1.8 direct-connect wind tunnel.

Important design criteria have also been investigated. The spacing between pressure transducers was found to be crucial in determining an accurate estimate of the shock location in the isolator. The transducers must be spaced at least as close as the desired command resolution. Furthermore, the execution speed of the shock localization algorithm must be sufficiently fast to ensure the controller is acting upon recent information. The resolution and speed of the chosen actuation method was also found to be an important factor in achieving satisfactory control performance. Without sufficient actuation resolution, the controller failed to regulate the shock to the desired position leading to sustained oscillations. Without sufficient actuation speed, closed-

loop control is possible for slow disturbances, but the controller will not be able to react to fast changes in the shock position. This could lead to an unstart condition, and as a result, a lack of sufficient actuation speed could cause the failure of a given control implementation.

Further work should be conducted to improve shock position regulation in the presence of large, fast disturbances. Also, research into an experimental implementation of tracking control could be conducted to determine if the shock's position could be forced to follow a reference trajectory in the presence of upstream or downstream disturbances. A dynamics-based controller may be able to accomplish these goals and could be designed and implemented following a set of thorough system identification experiments to determine the dynamics of the system.

Also, further research into methods of shock actuation may be conducted for closed-loop shock control experiments to demonstrate unstart prevention. In many cases, the unstart process can occur very quickly necessitating the use of large, fast control inputs. The electrical stepper motor utilized in this research was commanded at a frequency of 10 Hz, but the success of any control scheme can depend heavily on the bandwidth of the actuator. With faster actuators, a certain control implementation may be able to reliably prevent unstart from occurring even in the presence of large, high frequency disturbances which could not be achieved with the PD controller presented here.

# Bibliography


[1] Dean Andreadis. Scramjets integrate air and space. *The Industrial Physicist*, Vol. 10, 2004.

[2] Thomas A. Ward. *Aerospace Propulsion Systems*. John Wiley & Sons, 2010.

[3] J. L. Wagner, K. B. Yuceil, A. Valdivia, N. T. Clemens, and D. S. Dolling. Experimental investigation of unstart in inlet/isolator model in mach 5 flow. *AIAA Journal*, Vol. 47, 2009.

[4] M. Bolitho and J. Jacob. Active vortex generators using jet vectoring plasma actuators. In *SAE Technical Papers, 2008, Wichita Aviation Technology Congress and Exhibition*, 2008.

[5] M. A. Cappelli Seong-kyun Im, Hyungrok Do. Plasma control of an unstarting supersonic flow. In *17th AIAA International Space Planes and Hypersonic Systems Technologies Conference*, 2011.

[6] Agustin Valdivia. Active control of supersonic inlet unstart using vortex generator jets and wheeler doublet vortex generators. Master's thesis, The University of Texas at Austin, May 2008.

[7] J. R. Hutzel, D. D. Decker, R. G. Cobb, P. I. King, and M. J. Veth. Scramjet isolator shock train location techniques. In *49th AIAA Aerospace*

*Sciences Meeting*, January 2011.

[8] John R. Hutzel. *Scramjet Isolator Modeling and Control*. PhD thesis, Air Force Institute of Technology, December 2011.

[9] J. R. Hutzel, D. D. Decker, and J. M. Donbar. Scramjet isolator shock-train leading-edge location modeling. In *17th AIAA Internation Space Plance and Hypersonic Systems and Technologies Conference*, April 2011.

[10] Kelley E. Hutchins. Detection and transient dynamics modeling of experimental hypersonic inlet unstart. Master's thesis, The University of Texas at Austin, December 2011.

[11] K. E. Hutchins, M. Szmuk, N. T. Clemens, M. R. Akella, J. M. Donbar, and S. Gogineni. Transient dynamics modeling of experimental hypersonic inlet unstart. In *65th Annual Meeting of the APS Division of Fluid Dynamics*, Nov 2012.

[12] J. M. Ashley, M. Szmuk, N. T. Clemens, M. R. Akella, S. Gogineni, and J. M. Donbar. Closed-loop control of shock location in mach 1.8 direct connect wind tunnel. In *7th AIAA Flow Control Conference, AIAA Aviation and Aeronautics Forum and Exposition 2014*, June, 2014.

[13] National Instruments Corporation. Labview 2012 software package ver. 12.0, Austin, TX 2012.

[14] J. M. Donbar, G. J. Linn, S. Srikant, and M. R. Akella. High-frequency pressure measurements for unstart detection in scramjet isolators. In

*46th AIAA/ASME/SAE/ASEE Joint Propulsion Conference and Exhibit*, Nashville, TN, July 2010.

[15] D. Le, C. Goyne, and R. Krauss. Shock train leading-edge detection in a dual-mode scramjet. *Journal of Propulsion and Power*, 24(5), Sept-Oct 2008.

[16] G. L. Cole, G. H. Neiner, and M. J. Crosby. Design and performance of a digital electronic normal shock position sensor for mixed-compression inlets. *NASA Technical Note D-5606*, December 1969.

[17] M. O. Dustin, G. L. Cole, and R. E. Wallhagen. Determination of normal shock position in a mixed-compression supersonic inlet. *NASA Technical Memorandum X-2397*, November 1971.

[18] M. O. Dustin and G. L. Cole. Performance comparison of three normal-shock position sensors for mixed-compression inlets. *NASA Technical Memorandum X-2739*, March 1973.

[19] M. O. Dustin, G. L. Cole, and G. H. Neiner. Continuous-output terminal-shock-position sensor for mixed-compression inlets evaluated in wind-tunnel tests of yf-12 aircraft inlet. *NASA Technical Memorandum X-3144*, December 1974.

[20] M. Sajben, J. F. Donovan, and M. J. Morris. Experimental investigation of terminal shock sensors for mixed-compression inlets. *Journal of Propulsion and Power*, 8(1), Jan-Feb 1992.

[21] National Instruments. *LabVIEW PID and Fuzzy Logic Toolkit User Manual*, June 2009.